

Manganese ore exploration using electrical resistivity and induced polarization methods in Central Belt, Peninsular Malaysia

Hussein Ahmed Hasan Zaid¹, Mohd Hariri Arifin¹, Hamzah Hussin²,
Mohd Basril Iswadi Basori¹, Mohd Rozi Umor¹ and Suraya Hilmi Hazim¹

¹Programme Geology, Department of Earth Sciences and Environmental, Universiti Kebangsaan Malaysia, Bangi, Selangor, Malaysia, and ²Program Geosains, Jabatan Geosains, Fakulti Sains Bumi, Universiti Malaysia Kelantan, Jeli, Kelantan 17600, Malaysia

Received May 2021, revision accepted February 2022

ABSTRACT

Geophysical survey techniques were carried out to identify the potential zones of manganese ore in Central Peninsular Malaysia. Electrical resistivity tomography and induced polarization (IP) geoelectrical methods have been used to identify the metal distribution and mineralization zones. Five geoelectrical survey profiles were deployed at the proposed site using pole-dipole array in the W-E direction with lengths of 400 m and 800 m. The results of the resistivity and IP inversion indicate the presence of well-correlated low resistivity ($\leq 200 \Omega\text{m}$) and high chargeability zones ($\geq 10 \text{ms}$) embedded in the varied weathered host rock as massive and disseminated ore bodies. The 3-D maps generated enabled the delineation of the conductive bodies orientation and mineral of interest distribution. Results of the geochemical analysis contributed to validating the site as a potential mineralized zone with a high concentration of manganese. The study suggests further geophysical investigations in the southern segment of the research area to produce a more consistent image of the subsurface structures, and conclusively identifying the extension of mineral deposits for the purpose of ore prospecting to aid drilling operations.

Key words: Electrical resistivity tomography, Gua Musang, Induced polarization, Kelantan, Manganese ore, Peninsular Malaysia.

INTRODUCTION

Malaysia is endowed with a rich variety of ore deposits, particularly in the Central Belt of Peninsular Malaysia (Scrivenor, 1928), and is anticipated to remain on the path of mining development, motivated by the continued demand for mineral resources, notably manganese, iron, gold, tin, and other metallic ores (e.g. Majid et al., 2013; Kusin et al., 2017).

Manganese is a ferrous ore with growing significance in steel industries worldwide for the purpose of production of various alloys, thereby depriving low- and high-grade deposits and encouraging the prospect of such ore deposits (Ramazi and Mostafaie, 2013; Ismail et al., 2016). However, the pro-

cess of formation and deposition of manganese ores requires various geological conditions that were initially formed from ancient marine sedimentary rocks, and as a result of subsequent tectonic uplifts and erosions, these deposits have been exposed above the continent (Schulz et al., 2018). Studies investigating the geology of the Central Belt by the Malaysian Department of Minerals and Geosciences have shown that most of mineral deposits, e.g. base metals deposits, occur within Permo-Triassic metasedimentary rocks (e.g., Hutchison, 2007; Basori et al., 2016). The study area is located in the Central Belt of Peninsular Malaysia, and there is a strong motivation to investigate the potential occurrence of manganese ores in the region.

The identification of subterranean geological conditions in mineral prospecting using traditional methods such as pit

E-mail: hariri@ukm.edu.my

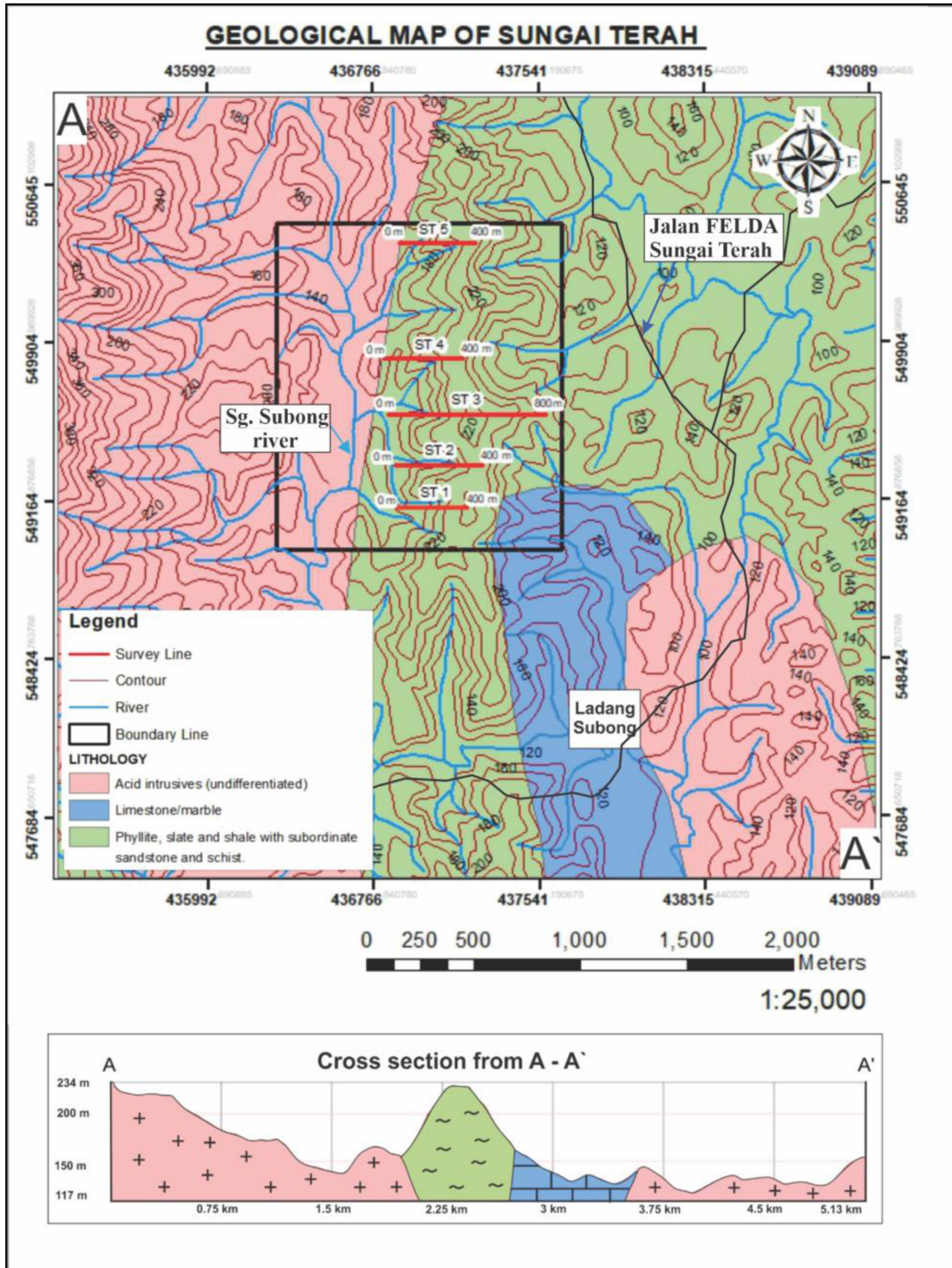


Figure 1 Geological map of the study site with inferred geological cross-section A-A'.

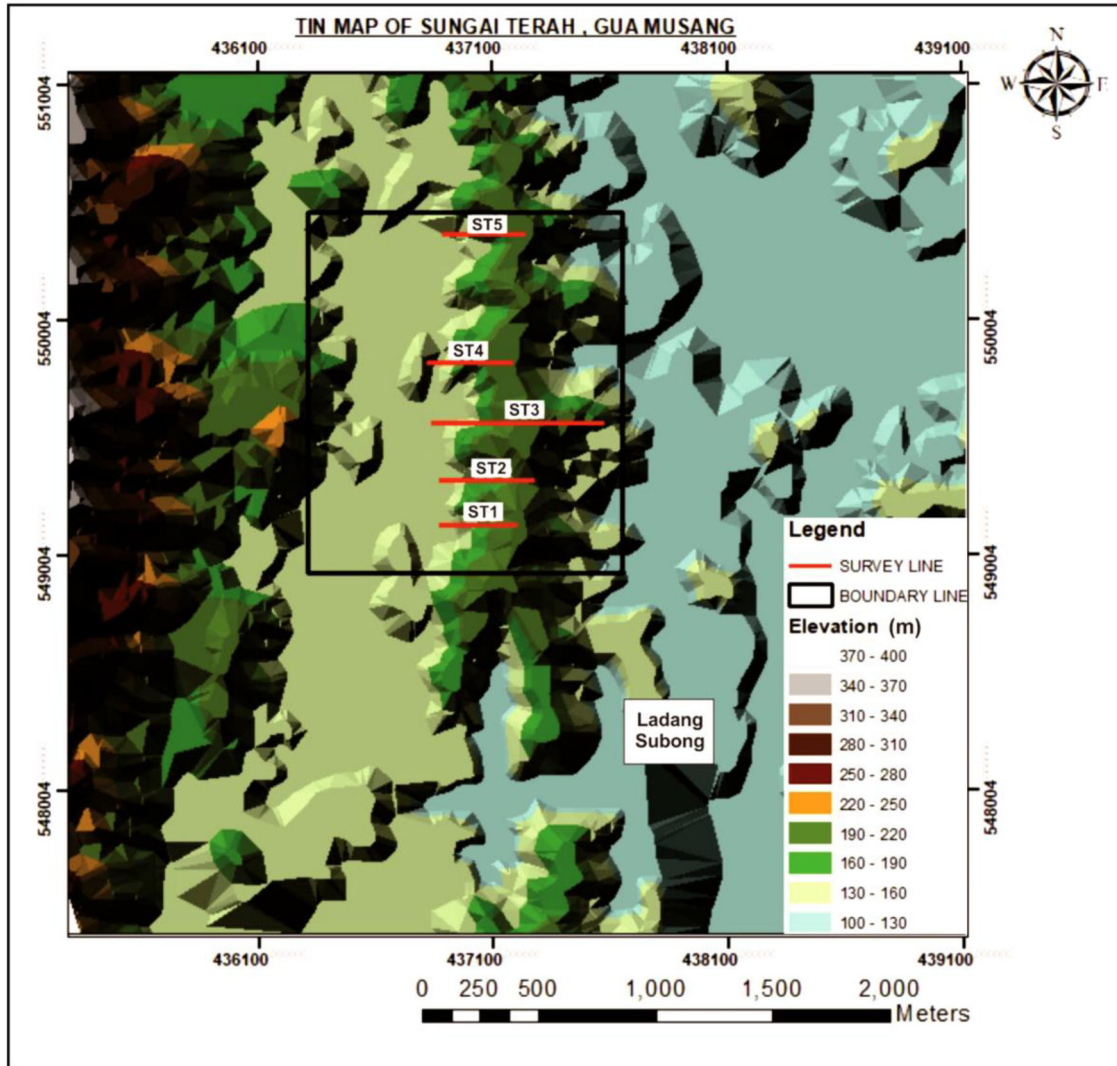


Figure 2 Map of study area at Ladang Sungai Terah, Gua Musang region, showing the 3-D elevation of deployed survey lines.

testing and drilling operations remains a major issue, with limited area coverage and little spatial observations over extremely complex formations (Corral and Earle, 2009). As a result of these issues, geophysical prospecting approaches have been used as alternative tools, some of which are scalable, and which provide spatial continuous detection of physical property sources with their changes (e.g., Day-Lewis et al., 2017; Power et al., 2018). Selection of such techniques for the purposes of mineral exploration is controlled by the physical characteristics of mineral in the ore bodies, their host rocks, the geological setting and the topographical parameters (Sultan

et al., 2009; Ramazi and Mostafaie, 2013; Gurin et al., 2015; Zhang et al., 2018).

Geoelectrical investigations have proven to be an effective geophysical method for delineating mineralized structure regions (Riva et al., 2019). The integration of electrical resistivity tomography (ERT) and induced polarization (IP) in geoelectrical methods is extensively applied in detailed surveys of geochemical parameters for the delineation base metals deposits (Moreira et al., 2020). Notwithstanding the simultaneous application of such approaches in mineral exploration, these methods are also used in a wide variety of environmen-

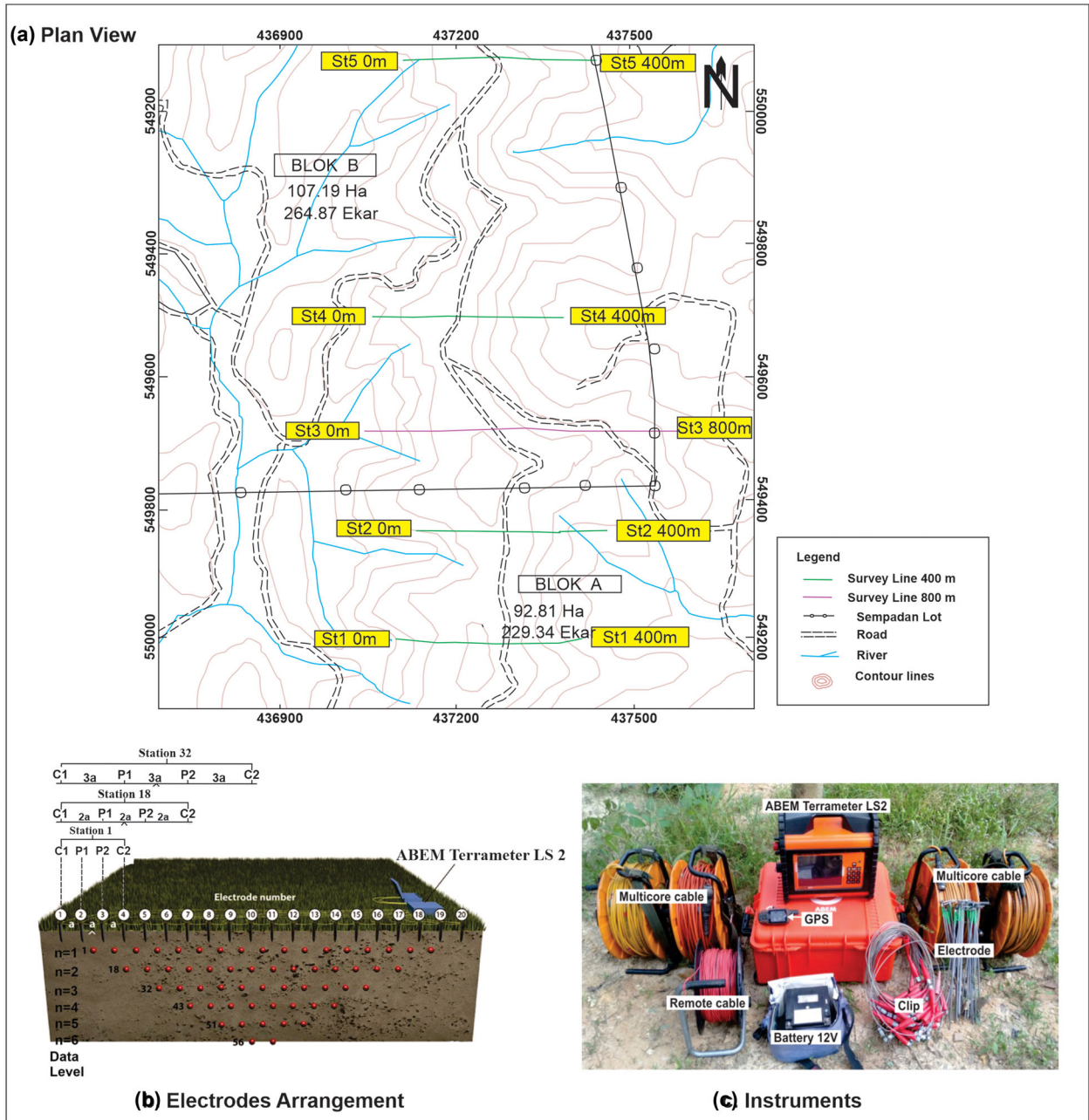


Figure 3 (a) Location of ERT-IP survey lines indicated in plan view; (b) geoelectrical data acquisition electrodes arrangement exhibiting the measurement sequence to construct pseudo-sections (Loke et al., 2013); (c) equipment and tools used for the data acquisition of ERT-IP subsurface manganese deposits.

tal and hydrogeological studies as well (e.g., Revil et al., 2012; Loke et al., 2013; Binley et al., 2015; Rosolen et al., 2019).

Electrical resistivity prospecting surveys are among the oldest and most widely applied geophysical methods (Reynolds, 2011). It has been typically used in exploration

surveys of mineral deposits (Bauman, 2005; Legault et al., 2008). The IP approach is generally performed for this type of investigation due to the high chargeability values of metals distributed in the geological formations and has been developed and mainly designed for the recognition of

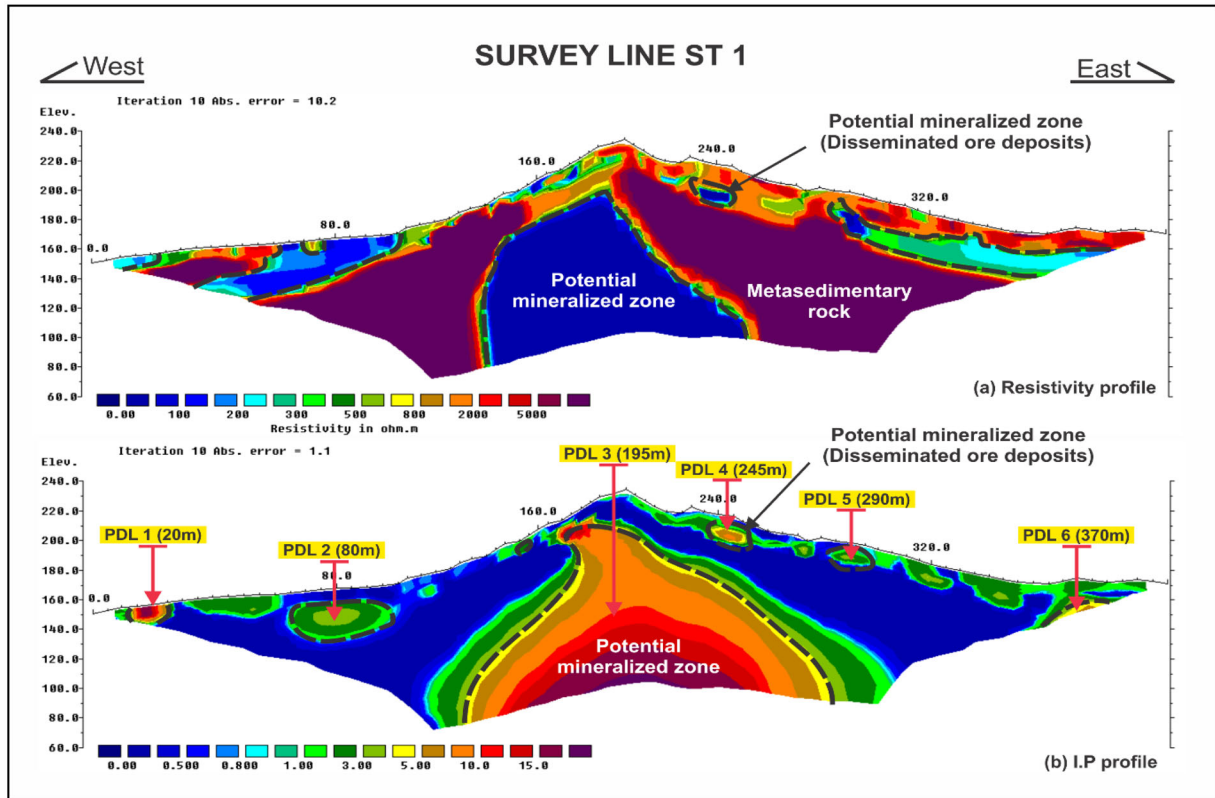


Figure 4 Interpreted resistivity and chargeability sections inverted from ERT and IP data for line ST 1.

disseminated sulphides (Moreira et al., 2014; Vieira et al., 2016).

Many research works have been conducted using the geophysical methodologies for manganese exploration with variable success. The combination of ERT and IP methods was performed to investigate the supergene manganese ore deposits in south-eastern Brazil (Moreira et al., 2014). Similarly, Srigutomo and Pratomo (2016) used these techniques for exploration of manganese ore in an unknown area. Other studies have combined various geophysical methods, for instance Ramazi and Mostafaie (2013) applied resistivity, IP and self-potential (SP) techniques to prospect and evaluate the manganese ore in Marand, Iran. More recently, Araffa et al. (2020) deployed three geophysical techniques, including magnetic, IP and resistivity, for mapping of manganese-iron deposits at Wadi Al Sahu area, Sinai, Egypt.

The main objective of this study has been to analyse the effectiveness of ERT and IP (a combination of geophysical and geoelectrical methods) as exploration tools to locate manganese prospects in Central Peninsular Malaysia. This study will provide greater insight on the existence, shape, and depth of the manganese ores beneath the subsurface as informed by

the data collected on-site using the combination of ERT and IP methods.

GEOLOGICAL SETTING OF THE STUDY AREA

The study area is located at Ladang Sungai Terah (LST), Gua Musang, Kelantan, between the latitudes $4^{\circ}57'48.41''\text{N}$ to $4^{\circ}58'34.42''\text{N}$ and longitudes $101^{\circ}55'6.68''\text{E}$ to $101^{\circ}55'48.03''\text{E}$, which is part of the Central Belt of Peninsular Malaysia. The area can be accessed by Jelawang-Gua Musang road, about 12 km from the Gua Musang district (Fig. 1). The topography is characterized by hilly terrains gridded by the West Malaysia (RSO), using datum system of the Kertau 1948 with an elevation profile varying between 171 m and 250 m from north to south relative to mean sea level. Figure 2 illustrates the 3-D topography of the research area, including the geoelectrical line directions. The occurrence of well-exposed rock outcrops is very rare on-site as the area is predominantly covered by rubber and oil palm trees.

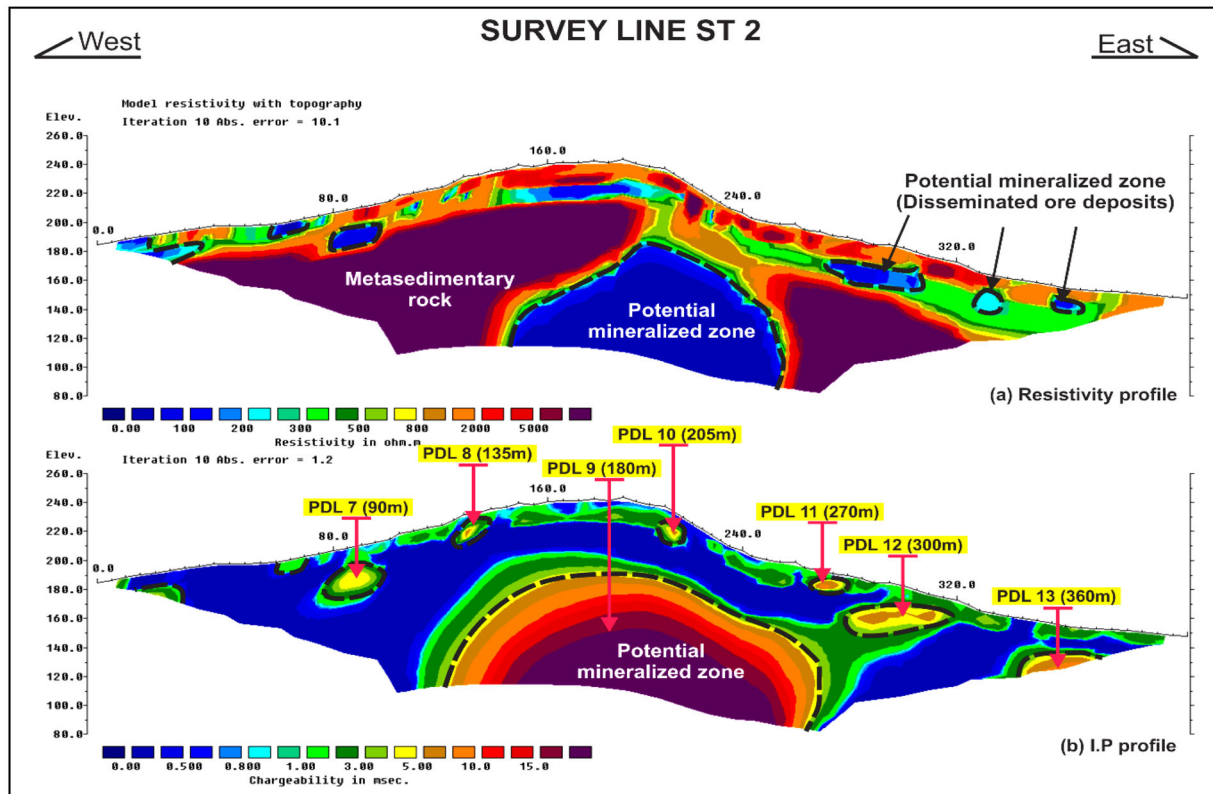


Figure 5 Interpreted resistivity and chargeability sections inverted from ERT and IP data for line ST 2.

Regional geology

The study area is part of the Central Belt of Peninsular Malaysia. Metcalfe (2013), Zaw et al. (2014) and Basori et al. (2016) suggested that the Central Belt represents the Permian volcanic arc, which formed along the margin of the East Malaya Block. According to Macdonald (1967), Heng et al. (2006) and Arifin et al. (2019), rocks in the study area consist of Permo-Triassic sedimentary rocks (mainly argillaceous-arenaceous sediments and calcareous intercalation), and were later intruded by the Triassic granitoids (Fig. 1). The manganese occurrence in the LST region has been neither studied in detail nor seen intense exploration activity. However, a brief description of the LST and other manganese occurrences in Central Belt (north Gua Musang) has been given by Macdonald (1967). Ongoing geological, geochemical and geophysical work in the area has also provided more information on the occurrence of manganese ore. The manganese ore can be found as discontinuous lenses and is hosted by metasedimentary rocks, consisting of phyllite and slate. In the southern part of the survey area, a series of micritic limestone bodies were observed and may consist of preserved fossils such as

foraminifera, bivalves and brachiopods. The prevailing structural trend is oriented N-S with manganese mineralization following the same orientation. The LST manganese ore is found to contain nearly 42 wt% manganese metals as measured by X-ray fluorescence analysis (Table 1).

MATERIALS AND METHODS

Electrical resistivity tomography and induced polarization techniques

Electrical resistivity tomography (ERT) is a direct current (DC) technique developed to image the resistivity pattern of the subsurface using multi-electrode systems (Griffiths and Baker, 1993). Measurements of ERT are conducted by injecting a DC through the ground with two transmitter current electrodes C1 and C2 to generate an electrical circuit, and recording the resulting variations in electrical potential (ΔV) across two other receiver potential electrodes P1 and P2. The measured potential differences are converted to apparent resistivity (ρ_a) in units of ohm-m (Riva et al., 2019). The results of such methods depend on the arrangements of electrodes or

Table 1 Quantitative analysis of elements in manganese ore sample from southern of Kelantan using the X-ray fluorescence method

Detected Elements		Manganese (Mn)	Iron (Fe)	Titanium (Ti)	Potassium (K)	Barium (Ba)	Zinc (Zn)	Calcium (Ca)	Arsenic (As)
Results (%)	Maximum	41.24	1.64	0.04	0.05	2.40	0.035	0.49	0.060
	Minimum	41.34	1.67	0.06	0.07	2.70	0.040	0.53	0.065

Table 2 Characteristics of the acquired ERT and IP profiles using pole–dipole configuration

Acquisition date	Profile	Origin coordinates	End coordinates	Total length (m)	Electrode spacing (m)	Parameter measured ^a	Estimated maximum depth (m)
10th to 12th January 2020	ST 1	437156 E 549163 N	437370 E 54145 N	400	5	ρ_a, M	100
	ST 2	437038 E 549392 N	43447 E 549363 N	400	5	ρ_a, M	100
	ST 3	436988 E 549612 N	437737 E 549569 N	800	10	ρ_a, M	200
	ST 4	437015 E 549869 N	437345 E 549914 N	400	5	ρ_a, M	100
	ST 5	437058 E 550451 N	437411 E 550407 N	400	5	ρ_a, M	100

^a ρ_a (apparent resistivity) and M (chargeability) are obtained from ERT and IP survey, respectively.

the response of physical properties to the DC applied (Loke, 2004; Upadhyay et al., 2020).

IP is a current-stimulated electrical phenomenon observed as a delayed voltage response in earth materials (Sharma, 1997). IP methods are deployed in a comparable approach to DC resistivity techniques. On the other hand, this approach was used to determine the chargeability M (in ms), which demonstrates the magnitude of electrical polarization effects (i.e., ability to store electrical charge) experienced by ions in the vicinity of metallic minerals within rocks (e.g., Spitzer and Chouteau, 2003). As the transmitted electrical current into the ground is interrupted, the voltage gradually decays over time across the potential electrodes to zero. This voltage decay study is manifested as time-domain IP (TDIP) and is connected to the presence of either clay minerals in the weathered regions or conductive minerals in rocks (Martínez et al., 2019).

The survey profiles were arranged in a W–E direction, which intersects perpendicularly to the regional structure orientation, i.e. the N–S direction of Kelantan. Other affecting factors for the design and surveying of the lines were the observed indicators of mineralization in the field; small outcrops of the lenses of manganese mineral disseminated within the phyllite and slate metasedimentary rocks in the centre of the study area, located mostly according to the setting of regional

structural geology of the area. Each survey line started at a specified location and traversed along the terrain and plateau of area over a distance of 400 m before ending at the opposite location. Line ST 3 was extended further than the other lines to reach 800 m in length so as to acquire the electrical data of the exposed mineral bodies in the centre of area. Both methods (ERT and IP) rely on the placement of several electrodes along a survey line connected to a multi-core cable. The distance between electrodes controls the degree of lateral and vertical resolution, while the spread length of the configuration array limits the maximum investigation depth. In order to maximize the model resolution, the electrodes need to be placed closer together (Martínez et al., 2019). The recorded ERT and IP anomalies have a good correlation with mineral body outcrops, demonstrating the effectiveness of the used geoelectrical methods for manganese mineral exploration.

Acquisition and inversion of datasets

Geoelectrical data acquisition for subsurface properties was carried out by using a resistivity metre system integrated with a built-in programmable microprocessor (ABEM Terrameter LS2), which automatically identifies the specific four stainless metal steel electrodes within each measurement without any

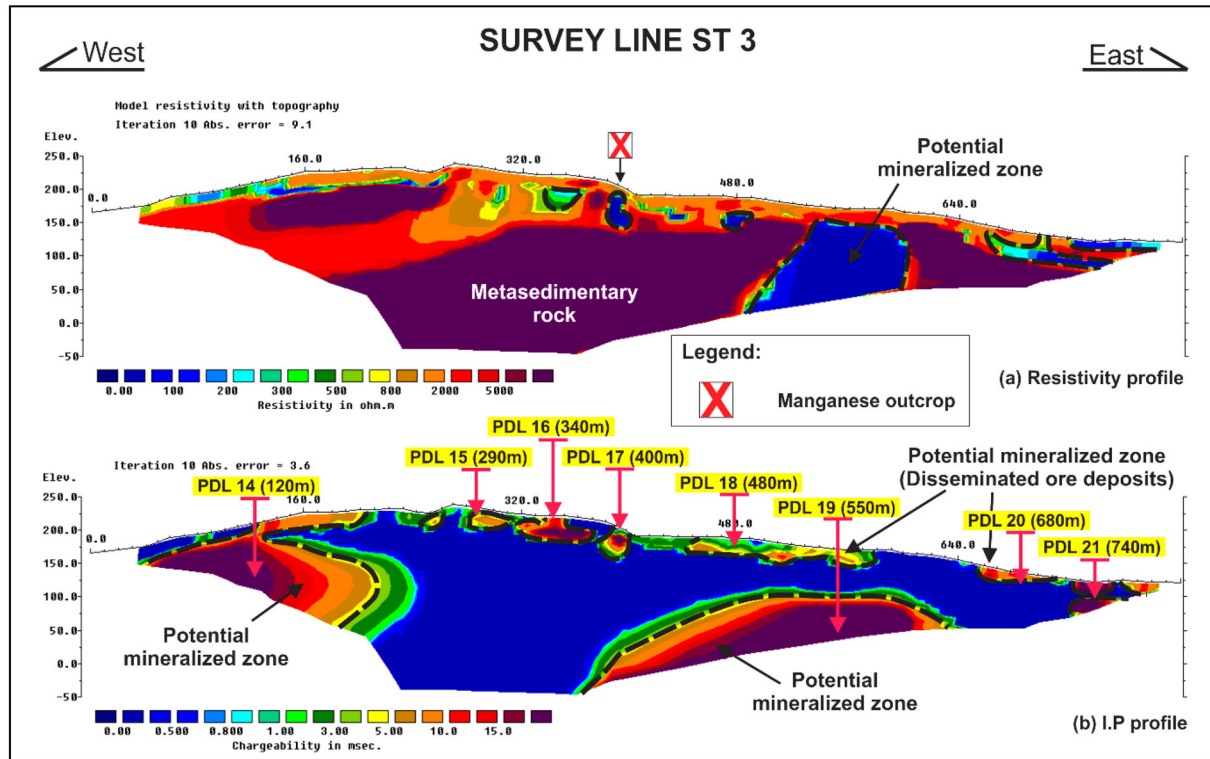


Figure 6 Interpreted resistivity and chargeability sections inverted from ERT and IP data for line ST 3.

human interference (Fig. 3). The pole–dipole array with unit electrode spacing of 5 and 10 m (Table 2) were used to obtain the apparent resistivity and apparent chargeability measurements as this approach produces better lateral and vertical resolution (Dahlin and Zhou, 2004; Arifin et al., 2019; Kayode et al., 2019). Figure 3(b) shows the electrode arrangement and sequence measurement to construct a pseudo-section. A total of 5 parallel electrical survey lines were deployed with lengths of 400 m and 800 m. The survey lines were set up in the W–E direction, positioned generally perpendicular to the trend of main geological structures on-site to provide consistent datasets for manganese exploration. A direct current (DC) supplied by a 12-V battery was driven into the ground by using 41 to 61 stainless steel metal electrodes connected by jumpers to two reels of 200 m multi-core electrical cables and the potential difference measured is recorded through the potential electrodes. The location and elevation of the electrodes along every survey line were geo-referenced using a portable global positioning system (GPS) to synchronize the data for processing and inversion procedure.

Inversion modelling of the apparent resistivity and chargeability data was performed using RES2DINVx64 tomography inversion software. Prior to inversion, a topo-

graphic correction was incorporated, and any data affected by noise were filtered out. The inversion algorithm used the constrained least-squares technique based on the robust finite element method to generate a calculated model that emphasizes true resistivities of subsurface geological features (Loke et al., 2006). Root mean square errors of inverted data for lines ST 1, 2, 3, 4 and 5 were less than 11%, after a maximum of ten iterations for the acquired lines. The 2-D inverted results were again tabulated and processed using Oasis Montaj software, from Geosoft, combined with GPS data obtained at the position of each electrode to develop a 3-D visualization model for better understanding of the complex geological structure. The previously inverted data was interpolated using a minimal curvature algorithm.

RESULTS

2-D electrical resistivity tomography and induced polarization models

Figure 4 illustrates the inverted resistivity and chargeability section obtained along the geophysical survey line ST 1 in the southern part of the study area. The resistivity image shows

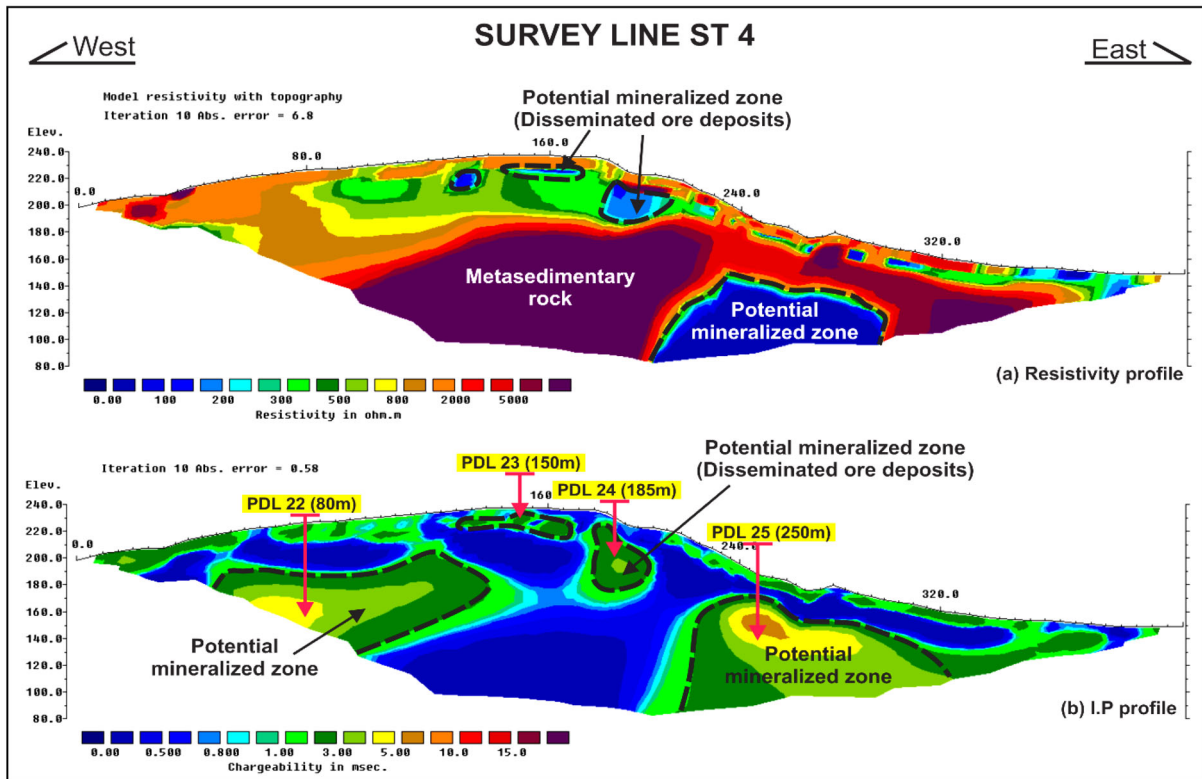


Figure 7 Interpreted resistivity and chargeability sections inverted from ERT and IP data for line ST 4.

a main massive low resistivity zone at the centre of this survey line between 130 m and 205 m with a delineated resistivity value of less than 170 Ωm , as indicated by black dashed lines shown in Figure 4a, while high resistivities of surrounding host rock were greater than 800 Ωm . Other multiple conductive subsurface features were distinguished within a depth of between approximately 5 m and 25 m. Figure 4(b) shows that the high chargeability values measured are greater than 10 ms, at a distance of 110 m to 270 m, well compatible with low resistive zones described above.

The results of the electrical resistivity tomography (ERP) and induced polarization (IP) survey line derived from data measured along line ST 2 with a total length of 400 m (Fig. 5) showed a significant similarity in the characteristics of resistivity and IP response compared to line ST 1. The major conductive feature is also detected in the middle of this profile with a higher depth varying from about 35 m down to 100 m, at a distance between 150 m and 205 m from the starting point of the survey line. As shown in Figure 5(a and b), the values of resistivity and chargeability for the conducting bodies are less than 200 Ωm and greater than 5 ms, respectively. These bodies are well correlated, and the values recorded for the surround-

ing regions correspond well to basement rocks, with resistivity measured to be greater than 2000 Ωm and chargeability less than 1.0 ms.

Figure 6 presents the inversion imaging of ERT and IP data obtained along line ST 3 (profile 3), which was the longest line covering a total length of nearly 800 m in the central part of the study area. The massive low resistivity anomaly was observed in the eastern part of this profile. This line was positioned close to the outcrop of manganese mineral ore exposure. The chargeability section model (Fig. 6b) shows that the estimated depth of these manganese ore outcrops is approximately 40 m down from the ground surface. Field observations reveal that the manganese ores are associated with slate as a host rock. The location of the electrical routing lines allowed the contrast region of subsurface physical properties detected in inversion models to be linked with zones of mineral concentrations (Moreira et al., 2014). Likewise, line of ST 3, similar massive conducting bodies were observed in the east of profile line ST 4 with resistivity below 200 Ωm and chargeability values of above 3 ms (Fig. 7a and b). Meanwhile, the correlated regions with high resistivity of greater than 2000 Ωm and a moderate to high chargeability ranging from 3 ms to

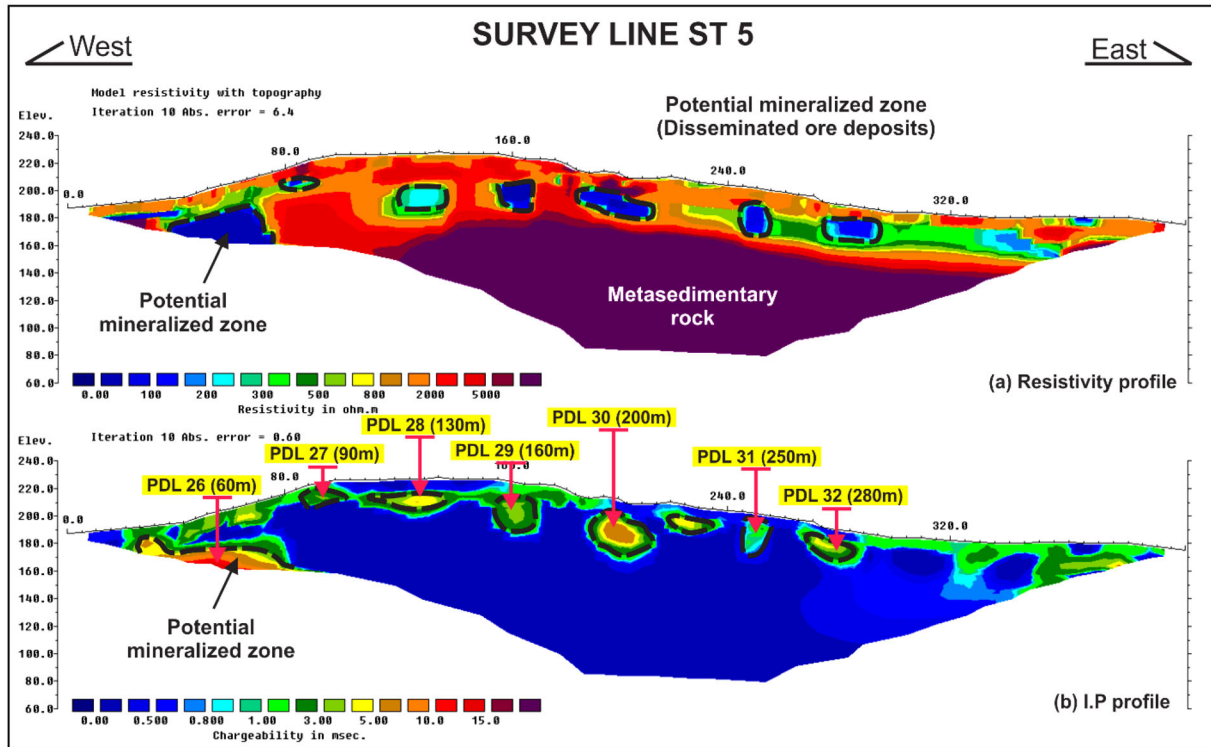


Figure 8 Interpreted resistivity and chargeability sections inverted from ERT and IP data for line ST 5.

15 ms may be interpreted as potential mineralized zones with a low concentration of ore deposits hosted in slightly weathered rocks.

The resistivity and chargeability data acquired from the geoelectrical survey line ST 5 (Fig. 8) do not show any indication of the presence of massive conducting bodies. However, multiple disseminated low resistive anomalies were located near subsurface with varying depths from about 5 m down to 40 m. These low resistivity values (Fig. 8a) correspond to the high chargeability values of more than 5 ms (Fig. 8b), which may indicate the presence of manganese mineralization lenses that is likely to be hosted by highly weathered metasedimentary rocks.

Fence diagram generation

The fence diagram is produced from the 2-D resistivity and chargeability results and is plotted as shown in Figures 9 and 10 to illustrate the correlation of delineated potential mineralized features along all profiles (i.e., ST 1–5), which are predominantly elongated in the north–south direction. The extension of the very low massive resistivity/high

chargeability structures appears to be substantially consistent, i.e. N–S, along the measured profiles except for the profile generated by line ST 5, where there is no observable geoelectrical signal recorded. However, disseminated bodies of low resistivity and high polarized values are well defined and observed along all recorded lines.

Resistivity and chargeability maps

The 3-D Oasis Montaj model parameters produced from the inversion sections of resistivity and chargeability are significant for better correlation and characterization, as shown in Figures 11 and 12. Based on chargeability map (Fig. 11), the high chargeability values (red to purple colour marked with dashed line) indicate the presence of potential mineralization zones, which could be interpreted as deposits of manganese ore. These deposits are geographically dispersed over a broad scale at the west–east of line ST 3 and extend towards the south direction, i.e. ST 2 and ST 1. Figure 12 shows the resistivity map of the study area. The regions of low resistivity values with intersection of high chargeability values revealed in the maps probably correspond to the conductive rock bodies.

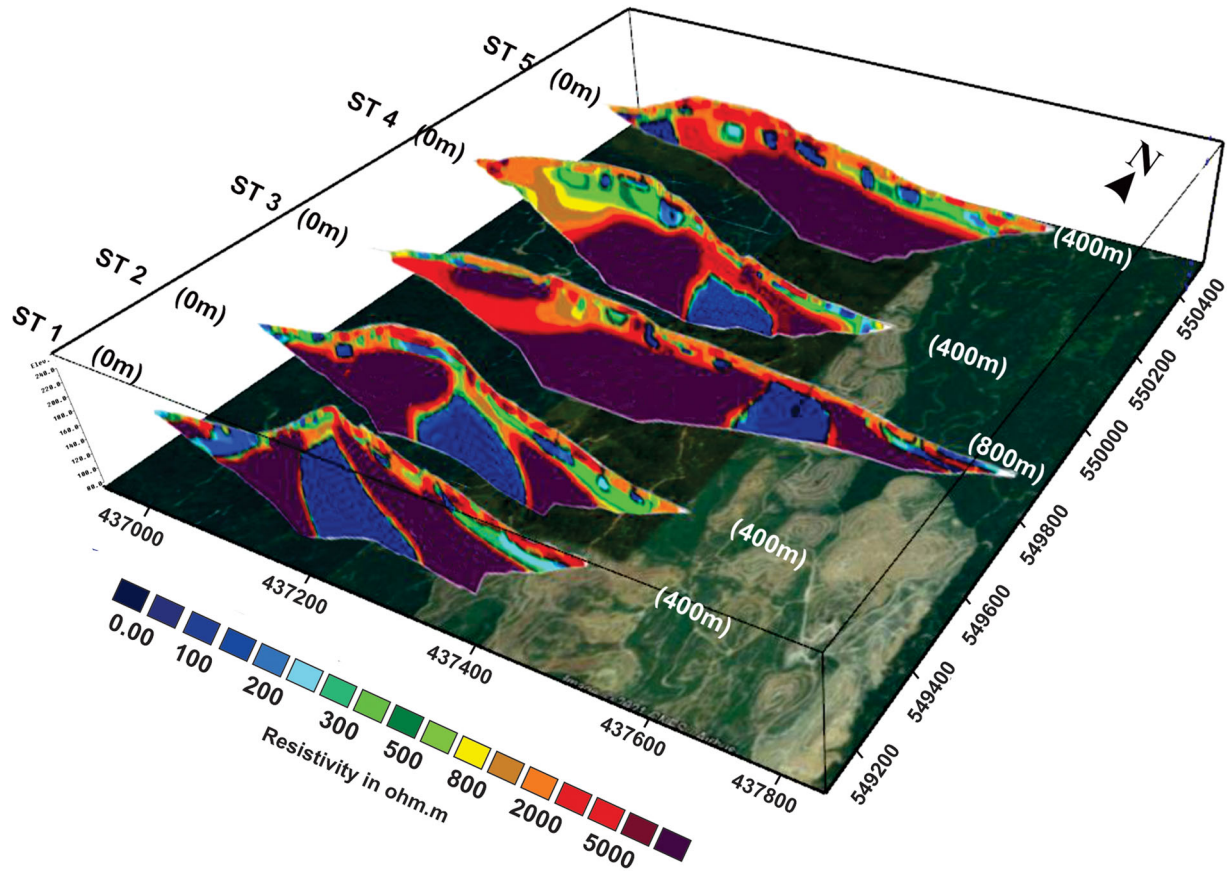


Figure 9 Aerial map of the research site showing the fence diagram of five resistivity survey lines joined together to identify the relation between 2D inversions.

DISCUSSION

Electrical geophysical measurements using electrical resistivity tomography (ERP) and induced polarization (IP) methods were explored to facilitate the delineation of the manganese ore reserve underlying the study area. The resistivity maps provide the highest resolution of the subsurface electrical properties of bedrock, which may reflect a strong connection to economic mineralization. Whereas the results of IP are useful to detect regions where conductive minerals are located within the host rock (e.g., Moon et al., 2006; Bery et al., 2012), the mineralization zones should have a high anomaly of chargeability in accordance with the fundamental IP theory (Telford et al., 1990). These anomaly measurements are then evaluated for the identification of aspect, size, distribution and structure as a starting point for the follow-up of detailed drilling exploration (Dentith and Mudge, 2014).

Analysis of the obtained resistivity and IP inversion models leads to remarkable anomalies as shown in Figures 4–8. Generally, the high-grade concentration of minerals for the

well-correlated values of low resistivity and high chargeability can be separated into two most significant anomalies types which could be defined as massive and disseminated subsurface earth materials underlying a specific area of interest. The massive conductive ore bodies observed at deeper higher-thickness levels, occupied most of the centre areas in sections ST 1 and 2, whereas the low massive resistivity features of models relevant to ST 3 and 4 were delineated in the western and eastern flanks of the research area. These conductive features are surrounded by bulky geology structures and could be described as hard basement rock, indicated by very high resistivity and low chargeability values. The geological setting and the described surficial lithology of the study area reflect a relationship between areas of high resistivity and the mineralized manganese associated with the slate rocks exposed at ground surface (e.g., ST 3 line).

In contrast, the disseminated anomalies are best developed at shallow depths along almost all reported surveyed lines where the anomalies are thinner and bound by

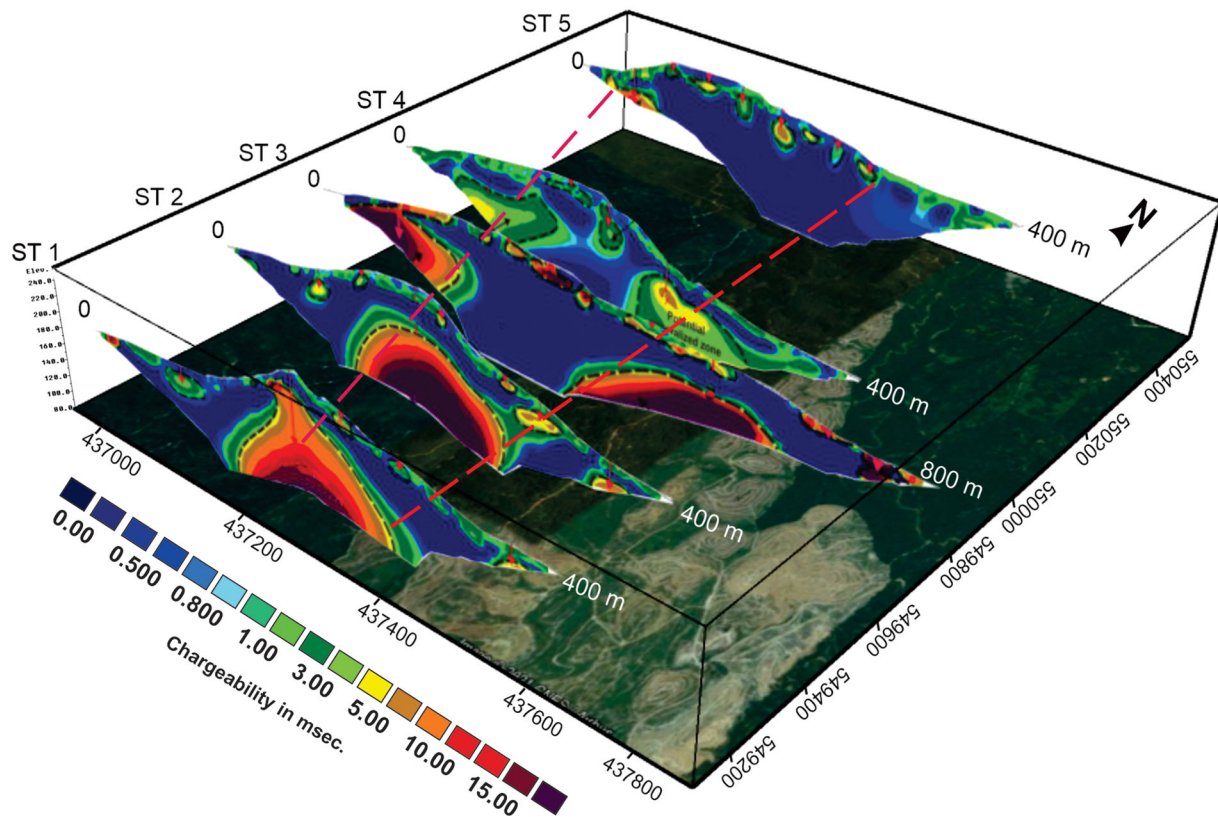


Figure 10 Aerial map of the project area presenting the high chargeability bodies, trending in approximately N–S direction as shown by dashed lines.

intermediate resistive structures. Such structures located near the subsurface are likely to be caused by the presence of clay soil, moisture and the weathering of shallow *in situ* metasedimentary rocks, which are predominantly composed of the slate and phyllite enclosing the manganese ore mineralized zones. These structures could be interpreted as host rock. Both of the massive and disseminated low resistivity inversion models primarily coincide with higher chargeability values of the IP inverted models. This is presumably due to the presence of bulky manganese ore, which reduces the electrical resistivity and increases the effect of chargeability. Comparing the results of chargeability among various studies is a challenging task, as it depends on the parameters of acquisition implemented. Studies by Vieira et al. (2016) and Casagrande et al. (2020) have shown similar or lower chargeability values for disseminated minerals. The X-ray fluorescence results of manganese ore analysis, obtained from the centre of line ST 1, show the presence of high-grade manganese, which can be correlated to the detected high chargeability response in the IP survey profile. High conductive targets were suggested for the follow-up of the drilling programme, as shown in Figure 13 and Table 3, with their coordinates and distances

noted, since they are likely to represent significant mineralized zones.

The ore pseudo-3D maps and fence diagrams of ERT and IP were produced for better understanding and recognition of orientation, possible spatial and lateral distribution of high resistivity and low chargeability locations, which serve as guidelines for the exploration of manganese deposits. Low resistivity structures showed an extensive horizontal continuity, i.e. ST 3 and 4, and elongation towards the line of ST 2 and 1 identified by N–S orientation with high chargeability association, as presented in Figures 11 and 12. Meanwhile, in the western regions of ST 3 and 4, high values of resistivity and the associated moderate to high chargeability values are interpreted as potential mineralization zones, but are likely to be below economic concentration ore, deposited in slightly weathered host rocks. In this case, however, the data interpolation between ST 4 and 5 using the algorithm method may not be accurate, since the vertical distance of about 500 m between these two lines is enormous, which may indicate that the mineralized zone, in the western portion of ST 5 line, appears to be isolated with no continuity in the uppermost north of study area.

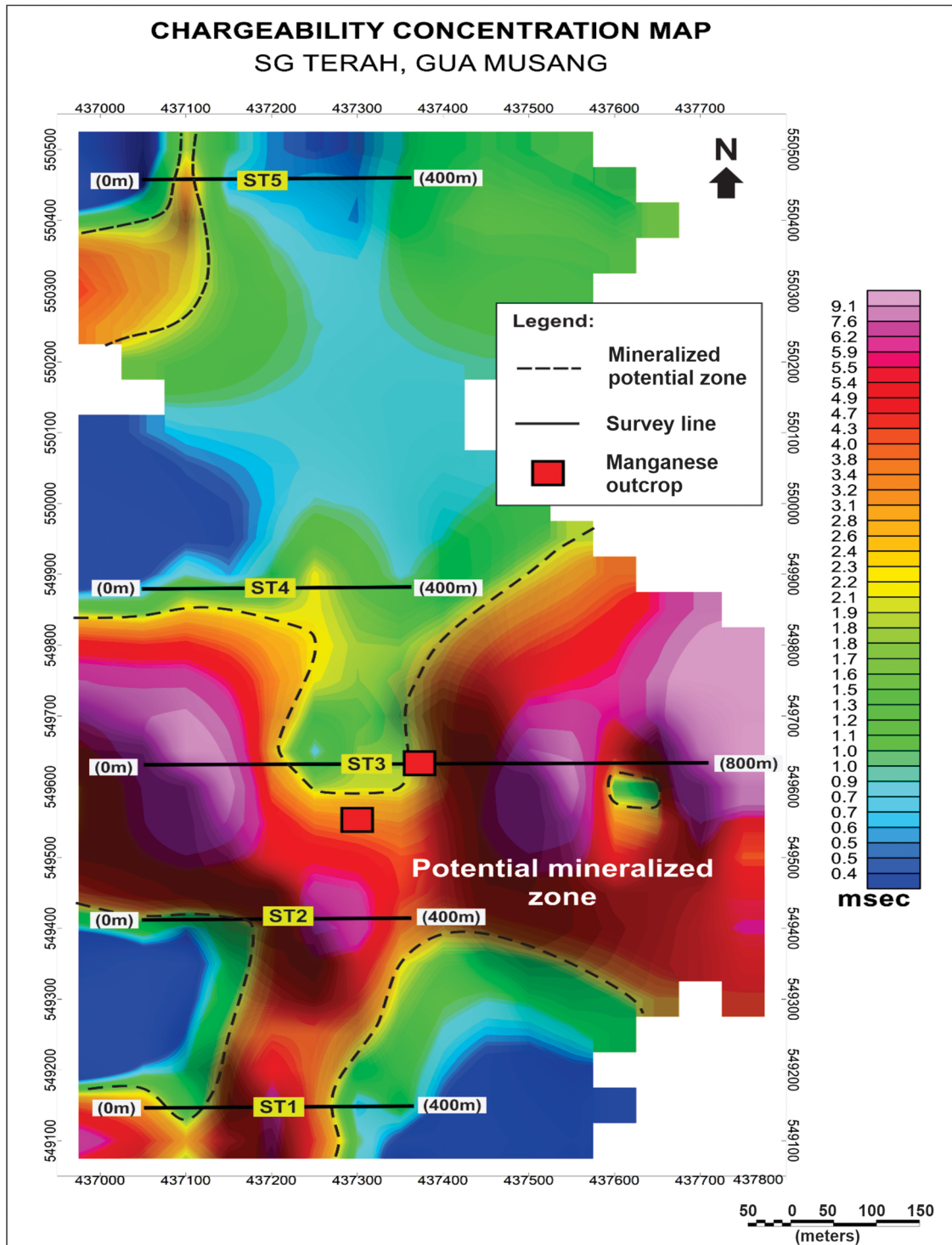


Figure 11 Pseudo-chargeability map showing the spatial extent and distributions of polarized bodies, i.e. the purple colour marked with dashed lines, and the manganese outcrops as indicated by red box.

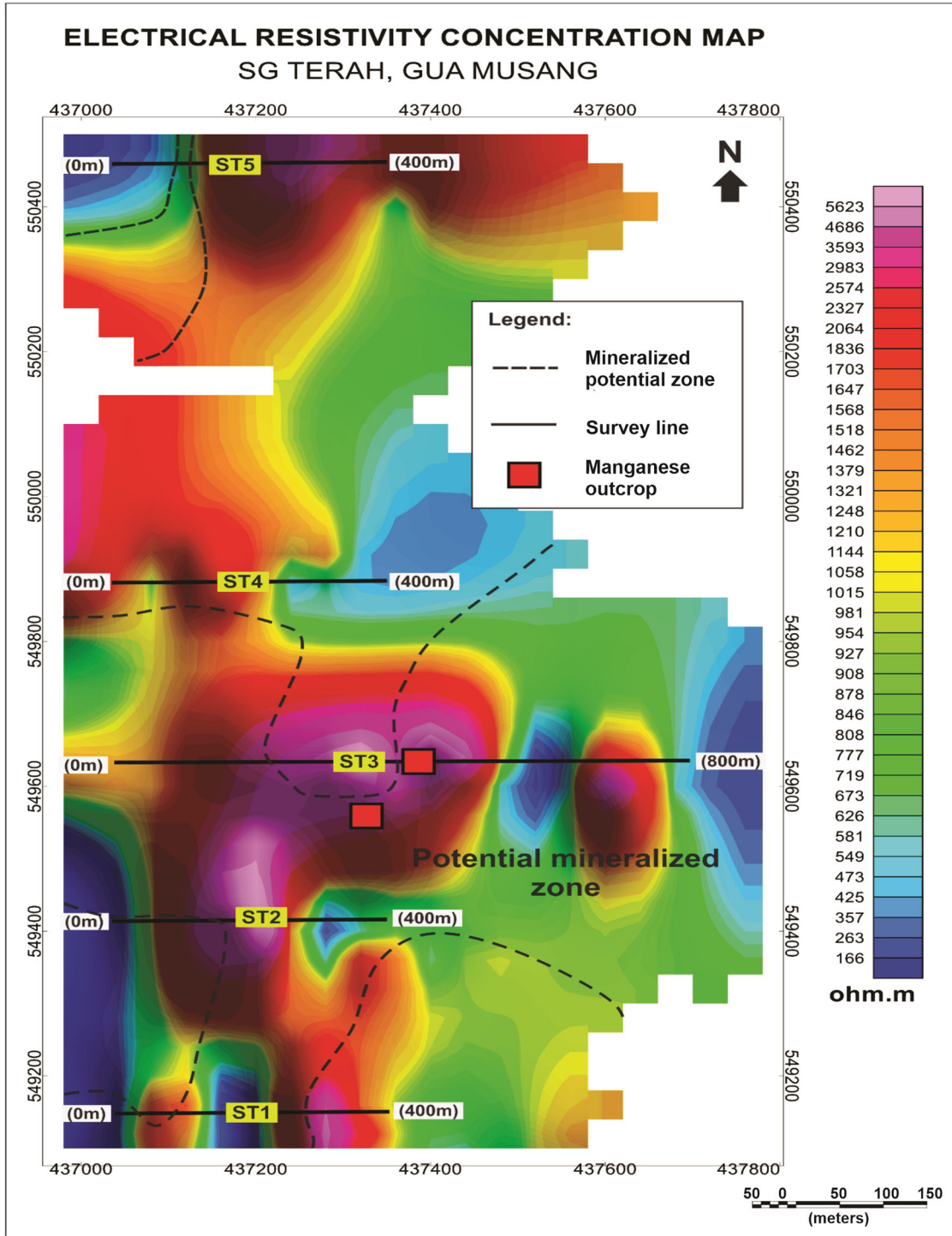


Figure 12 Pseudo-resistivity map showing the distribution of low resistive structures.

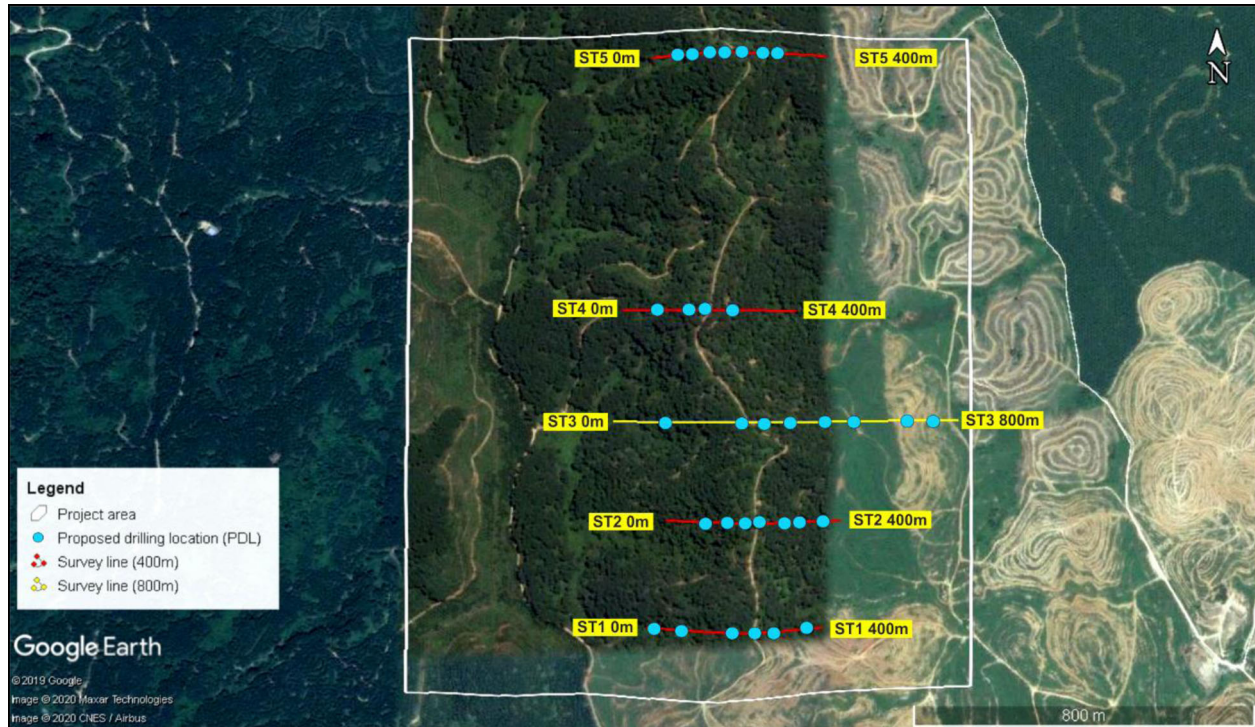


Figure 13 Aerial Google map of the study area shows the proposed locations of 32 borehole along each survey line.

This study, along with a few other studies in the same context, revealed the benefits of adopting integrated geophysical methods in preliminary research or the development of mining. Furthermore, the findings demonstrate that genetic models and regional tectonic evolution should be considered when conducting geophysical surveys in potentially mineralized zones.

CONCLUSIONS

This study uses a combination of survey and observation methods (electrical resistivity tomography (ERP) and induced polarization (IP)) to investigate the occurrence of manganese ore in Central Peninsular Malaysia. The profiles generated from the ERT-IP surveys successfully showcase the presence of highly conductive features associated with high chargeability values, enabling the pre-delineation of the potential manganese mineralization regions which help to inform and optimize probing processes in mineral exploration. The results of this study can be concluded as follows: (1) The presence of potential mineralized zones, in the form of massive and disseminated ore deposits located within fresh and highly weathered host rock, can be interpreted from regions of very low resistivity with high chargeability; (2) in the 3-D visualization models, data interpolation provides the possibility of delineating mineralized targets with clear contrasts between the physical properties of the subsurface along the survey lines, including the distinct distribution and orientation; and (3) a total of 32 borehole locations were proposed for follow-up drilling on the basis of the resistivity and chargeability distribution in subsurface of the study area.

This study demonstrates that the use of this ERT-IP technique is a highly effective diagnostic approach that makes it possible to delineate and identify both the lateral and depth extent of potential mineralized deposits. Further studies are strongly recommended in the southern part of the site to investigate the expanse of these deposits, including a further detailed analysis of the geochemical data which is important for confirmation of the results. Estimation through validation drilling or pitting near the outcrops or on the detected geophysical anomalies as the region is also under consideration for future mining projects.

Table 3 Proposed locations for the boreholes drilling programme

Line	Proposed drilling location (PDL)	Distance from 0 m of survey line (m)	Range of depth from surface layer (m)	Thickness of potential mineralized zone (m)	Easting (m)	Northing (m)
ST 1	PDL 1	20	0–10	10	437,149	549,168
	PDL 2	80	5–35	30	437,132	549,169
	PDL 3	195	10–100	90	437,197	549,167
	PDL 4	245	5–15	10	437,239	549,166
	PDL 5	290	5–15	10	437,279	549,150
	PDL 6	370	15–25	10	437,359	549,145
ST 2	PDL 7	90	10–35	25	437,114	549,394
	PDL 8	135	5–15	10	437,198	549,391
	PDL 9	180	35–100	65	437,241	549,390
	PDL 10	205	5–15	10	437,261	549,387
	PDL 11	270	5–15	10	437,314	549,378
	PDL 12	300	10–35	25	437,342	549,373
ST 3	PDL 13	360	20–40	20	437,406	437,406
	PDL 14	120	10–150	140	437,112	549,617
	PDL 15	290	5–30	25	437,258	549,632
	PDL 16	340	0–40	40	437,302	549,627
	PDL 17	400	0–40	40	437,368	549,635
	PDL 18	480	0–20	20	437,448	549,626
ST 4	PDL 19	550	0–20, 60–200	20, 140	437,513	549,620
	PDL 20	680	0–20	20	437,632	549,605
	PDL 21	740	0–50	50	437,687	549,591
	PDL 22	80	30–80	50	437,079	549,874
	PDL 23	150	5–20	15	437,135	549,882
	PDL 24	185	5–35	30	437,164	549,881
ST 5	PDL 25	250	20–100	80	437,224	549,897
	PDL 26	60	20–40	20	437,111	550,447
	PDL 27	90	5–15	10	437,131	550,450
	PDL 28	130	5–20	15	437,172	550,450
	PDL 29	160	5–25	20	437,197	550,449
	PDL 30	200	10–25	15	437,226	550,446
	PDL 31	250	5–25	20	437,269	550,442
	PDL 32	280	5–25	20	437,296	550,438

ACKNOWLEDGEMENTS

The authors wish to thank the staff members of Geo Technology Resources Sdn Bhd for their support in completing the acquisition and processing of data, and we also appreciate the thoughtful and constructive reviews of an anonymous reviewer due to significant contribution to the manuscript quality. Special thanks to the Geology program, Department of Earth Sciences and Environmental, Universiti Kebangsaan Malaysia staff for their insightful questions and comments.


DATA AVAILABILITY STATEMENT

The data that support the findings of this study are available from the corresponding author upon reasonable request.

ORCID

Hussein Ahmed Hasan Zaid 

<https://orcid.org/0000-0001-5100-2645>

Mohd Hariri Arifin 

<https://orcid.org/0000-0002-4231-6762>

Suraya Hilmi Hazim 

<https://orcid.org/0000-0002-1514-7529>

REFERENCES

- Araffa, S.A.S., Rabeih, T.T.T., Mousa, S.E.D.A.W., Nabi, S.H.A. and Al Deep, M. (2020) Integrated geophysical investigation for mapping of manganese-iron deposits at Wadi Al Sahu area, Sinai, Egypt—a case study. *Arabian Journal of Geosciences*, 13(17), 1–14. <https://doi.org/10.1007/s12517-020-05869-8>

- Arifin, M.H., Kayode, J.S., Izwan, M.K., Zaid, H.A.H. and Hussin, H. (2019) Data for the potential gold mineralization mapping with the applications of electrical resistivity imaging and induced polarization geophysical surveys. *Data in brief*, 22, 830–835. <https://doi.org/10.1016/j.dib.2018.12.086>
- Basori, M.B.I., Zaw, K., Meffre, S., Large, R.R. (2016) Geochemistry, geochronology, and tectonic setting of early Permian (~ 290 Ma) volcanic-hosted massive sulphide deposits of the Tasik Chini district, Peninsular Malaysia. *International Geology Review*, 58(8), 929–948. <https://doi.org/10.1080/00206814.2015.1136798>
- Bauman, P. (2005) 2-D resistivity surveying for hydrocarbons: a primer. *CSEG Recorder*, 30(4), 25–33.
- Bery, A.A., Saad, R., Mohamad, E.T., Jinmin, M., Azwin, I., Akip Tan, N. and Nordiana, M. (2012) Electrical resistivity and induced polarization data correlation with conductivity for iron ore exploration. *The Electronic Journal of Geotechnical Engineering*, 17, 3223–3233.
- Binley, A., Hubbard, S.S., Huisman, J.A., Revil, A., Robinson, D.A., Singha, K. and Slater, L.D., (2015) The emergence of hydrogeophysics for improved understanding of subsurface processes over multiple scales. *Water Resources Research*, 51(6), 3837–3866. <https://doi.org/10.1002/2015WR017016>
- Casagrande, M.F.S., Moreira, C.A. and Targa, D.A. (2020) Study of generation and underground flow of acid mine drainage in waste rock pile in an uranium mine using electrical resistivity tomography. *Pure and Applied Geophysics*, 177(2), 703–721. <https://doi.org/10.1007/s00024-019-02351-9>
- Corral, M.D. and Earle, J.L. (2009) *Gold Mining: Formation and Resource Estimation, Economics and Environmental Impact*. New York: Nova Science Pub Incorporated.
- Dahlin, T. and Zhou, B. (2004) A numerical comparison of 2D resistivity imaging with 10 electrode arrays. *Geophysical Prospecting*, 52(5), 379–398. <https://doi.org/10.1111/j.1365-2478.2004.00423.x>
- Day-Lewis, F.D., Slater, L.D., Robinson, J., Johnson, C.D., Terry, N. and Werkema, D. (2017) An overview of geophysical technologies appropriate for characterization and monitoring at fractured-rock sites. *Journal of Environmental Management*, 204, 709–720. <https://doi.org/10.1016/j.jenvman.2017.04.033>
- Dentith, M. and Mudge, S.T. (2014) *Geophysics for the Mineral Exploration Geoscientist*. Cambridge: Cambridge University Press.
- Gurin, G., Titov, K., Ilyin, Y. and Tarasov, A. (2015) Induced polarization of disseminated electronically conductive minerals: a semi-empirical model. *Geophysical Journal International*, 200(3), 1555–1565. <https://doi.org/10.1093/gji/ggu490>
- Griffiths, D.H. and Barker, R.D. (1993) Two-dimensional resistivity imaging and modelling in areas of complex geology. *Journal of Applied Geophysics*, 29(3-4), 211–226. [https://doi.org/10.1016/0926-9851\(93\)90005-J](https://doi.org/10.1016/0926-9851(93)90005-J)
- Heng, G.S., Hoe, T.G. and Hassan, W.F.W. (2006) Gold mineralization and zonation in the state of Kelantan. *Bulletin of the Geological Society of Malaysia*, 52, 143–152.
- Hutchison, C.S. (2007) *Geological Evolution of South-East Asia*. Kuala Lumpur. Geological Society of Malaysia.
- Ismail, S., Hashim, S.F.S., Hussin, H. and Abdullah, N.S. (2016) Chemical and mineralogical characterization of Malaysian low grade manganese ore. *Periodico di Mineralogia*, 85(3). <https://doi.org/10.2451/2016PM612>
- Kayode, J.S., Arifin, M.H., Kamarudin, M.K.A., Hussin, A., Nordin, M.N.M. and Roslan, N. (2019) The vulnerability of the aquifer units in the flood-affected areas of the east coast Peninsula Malaysia. *Arabian Journal of Geosciences*, 12(5), 1–18. <https://doi.org/10.1007/s12517-019-4323-2>
- Kusin, F.M., Abd Rahman, M.S., Madzin, Z., Jusop, S., Mohamat-Yusuff, F. and Ariffin, M. (2017) The occurrence and potential ecological risk assessment of bauxite mine-impacted water and sediments in Kuantan, Pahang, Malaysia. *Environmental Science and Pollution Research*, 24(2), 1306–1321. <https://doi.org/10.1007/s11356-016-7814-7>
- Legault, J.M., Carriere, D. and Petrie, L. (2008) Synthetic model testing and distributed acquisition dc resistivity results over an unconformity uranium target from the Athabasca Basin, northern Saskatchewan. *The Leading Edge*, 27(1), 46–51. <https://doi.org/10.1190/1.2831679>
- Loke, M.H. (2004) Tutorial: 2D and 3D electrical imaging surveys: Geotomo Software. Notes 128 pp. <http://www.alberta.ca>. [Accessed 23 July 2004].
- Loke, M.H., Chambers, J.E. and Ogilvy, R.D., (2006) Inversion of 2D spectral induced polarization imaging data. *Geophysical Prospecting*, 54(3), 287–301. <https://doi.org/10.1111/j.1365-2478.2006.00537.x>
- Loke, M.H., Chambers, J.E., Rucker, D.F. and Kuras, O., Wilkinson, P.B. (2013) Recent developments in the direct-current geoelectrical imaging method. *Journal of Applied Geophysics*, 95, 135–156. <https://doi.org/10.1016/j.jappgeo.2013.02.017>
- Macdonald, S. (1967) The geology and mineral resources of north Kelantan and north Trengganu (No. 10). *Geological Survey Headquarters*.
- Majid, A.A., Shaharudin, H.M., Alias, S. and Adnan, E., Hassan, A.I.A. and Ali, M.Z. (2013) Malaysian mining industry. *Minerals and Geoscience Department Malaysia*, Kuala Lumpur, 152.
- Martínez, J., Rey, J., Sandoval, S., Hidalgo, M. and Mendoza, R. (2019) Geophysical prospecting using ERT and IP techniques to locate Galena veins. *Remote Sensing*, 11(24), 2923. <https://doi.org/10.3390/rs11242923>
- Metcalfe, I., (2013) Gondwana dispersion and Asian accretion: Tectonic and palaeogeographic evolution of eastern Tethys. *Journal of Asian Earth Sciences*, 66, 1–33. <https://doi.org/10.1016/j.jseaes.2012.12.020>
- Moon, C.J., Whateley, M.K. and Evans, A.M. (2006) *Introduction to Mineral Exploration*. 2, India: Blackwell Publishing. https://www.academia.edu/4327228/Introduction_to_Mineral_Exploration_Second_Edition
- Moreira, C. A., Casagrande, M. F. S. and Borssatto, K. (2020) Analysis of the potential application of geophysical survey (induced polarization and DC resistivity) to a long-term mine planning in a sulfide deposit. *Arabian Journal of Geosciences*, 13(20), 1–12. <https://doi.org/10.1007/s12517-020-06096-x>
- Moreira, C.A., Rezende Borges, M., Lira Vieira, G.M., Malagutti Filho, W. and Fernandes Montanheiro, M.A. (2014) Geological and geophysical data integration for delimitation of mineralized areas

- in a supergene manganese deposits. *Geofísica Internacional*, 53(2), 199–210.
- Power, C., Tsourlos, P., Ramasamy, M., Nivorlis, A. and Mkandawire, M. (2018) Combined DC resistivity and induced polarization (DC-IP) for mapping the internal composition of a mine waste rock pile in Nova Scotia, Canada. *Journal of Applied Geophysics*, 150, 40–51. <https://doi.org/10.1016/j.jappgeo.2018.01.009>
- Ramazi, H. and Mostafaie, K. (2013) Application of integrated geoelectrical methods in Marand (Iran) manganese deposit exploration. *Arabian Journal of Geosciences*, 6(8), 2961–2970. <https://doi.org/10.1007/s12517-012-0537-2>
- Revil, A., Karaoulis, M., Johnson, T. and Kemna, A. (2012) Some low-frequency electrical methods for subsurface characterization and monitoring in hydrogeology. *Hydrogeology Journal*, 20(4), 617–658. <https://doi.org/10.1007/s10040-011-0819-x>
- Reynolds, J.M. (2011) *An Introduction to Applied and Environmental Geophysics*. Chichester: John Wiley & Sons.
- Riva, R., Ralay, R. and Boni, R. (2019) Evaluation of flake graphite ore using self-potential (SP), electrical resistivity tomography (ERT) and induced polarization (IP) methods in east coast of Madagascar. *Journal of Applied Geophysics*, 169, 134–141. <https://doi.org/10.1016/j.jappgeo.2019.07.001>
- Rosolen, V., Bueno, G.T., Mutema, M., Moreira, C.A., Junior, I.R.F., Nogueira, G. and Chaplot, V. (2019) On the link between soil hydromorphy and geomorphological development in the Cerrado (Brazil) wetlands. *Catena*, 176, 197–208. <https://doi.org/10.1016/j.catena.2019.01.022>
- Schulz, K.J., DeYoung, J.H., Seal, R.R., Bradley, D.C. (Eds.) (2018) *Critical Mineral Resources of the United States: Economic and Environmental Geology and Prospects for Future Supply*. Geological Survey.
- Scrivenor, J.B. (1928) *The Geology of Malayan Ore-Deposits*. London: Macmillan and Co.
- Sharma, P.V. (1997) *Environmental and Engineering Geophysics*. Cambridge: Cambridge University Press.
- Spitzer, K. and Chouteau, M. (2003) A dc resistivity and IP borehole survey at the Casa Berardi gold mine in northwestern Quebec. *Geophysics*, 68(2), 453–463. <https://doi.org/10.1190/1.1567221>
- Srigutomo, W. and Pratomo, P.M. (2016) 2D resistivity and induced polarization measurement for manganese ore exploration. *Journal of Physics: Conference Series*, 739 (1), 012138.
- Sultan, S.A., Mansour, S.A., Santos, F.M. and Helaly, A. S. (2009) Geophysical exploration for gold and associated minerals, case study: Wadi El Beida area, South Eastern Desert, Egypt. *Journal of Geophysics and Engineering*, 6(4), 345–356. <https://doi.org/10.1088/1742-2132/6/4/002>
- Telford, W.M., Telford, W.M., Geldart, L.P., Sheriff, R.E. and Sheriff, R.E., (1990) *Applied Geophysics*. Cambridge: Cambridge University Press.
- Upadhyay, A., Singh, A., Panda, K.P. and Sharma, S. P. (2020) Delineation of gold mineralization near Lawa village, North Singhbhum Mobile Belt, India, using electrical resistivity imaging, self-potential and very low frequency methods. *Journal of Applied Geophysics*, 172, 103902. <https://doi.org/10.1016/j.jappgeo.2019.103902>
- Vieira, L.B., Moreira, C.A. and Côrtes, A.R., Luvizotto, G.L. (2016) Geophysical modeling of the manganese deposit for Induced Polarization method in Itapira (Brazil). *Geofísica Internacional*, 55(2), 107–117.
- Zaw, K., Meffre, S., Lai, C.K., Burrett, C., Santosh, M., Graham, I. and Cromie, P. (2014) Tectonics and metallogeny of mainland Southeast Asia—a review and contribution. *Gondwana Research*, 26(1), 5–30. <https://doi.org/10.1016/j.gr.2013.10.010>
- Zhang, G., Lü, Q.T., Zhang, G.B., Lin, P.R., Jia, Z.Y. and Suo, K. (2018) Joint interpretation of geological, magnetic, AMT, and ERT data for mineral exploration in the Northeast of Inner Mongolia, China. *Pure and Applied Geophysics*, 175(3), 989–1002. <https://doi.org/10.1007/s00024-017-1733-5>